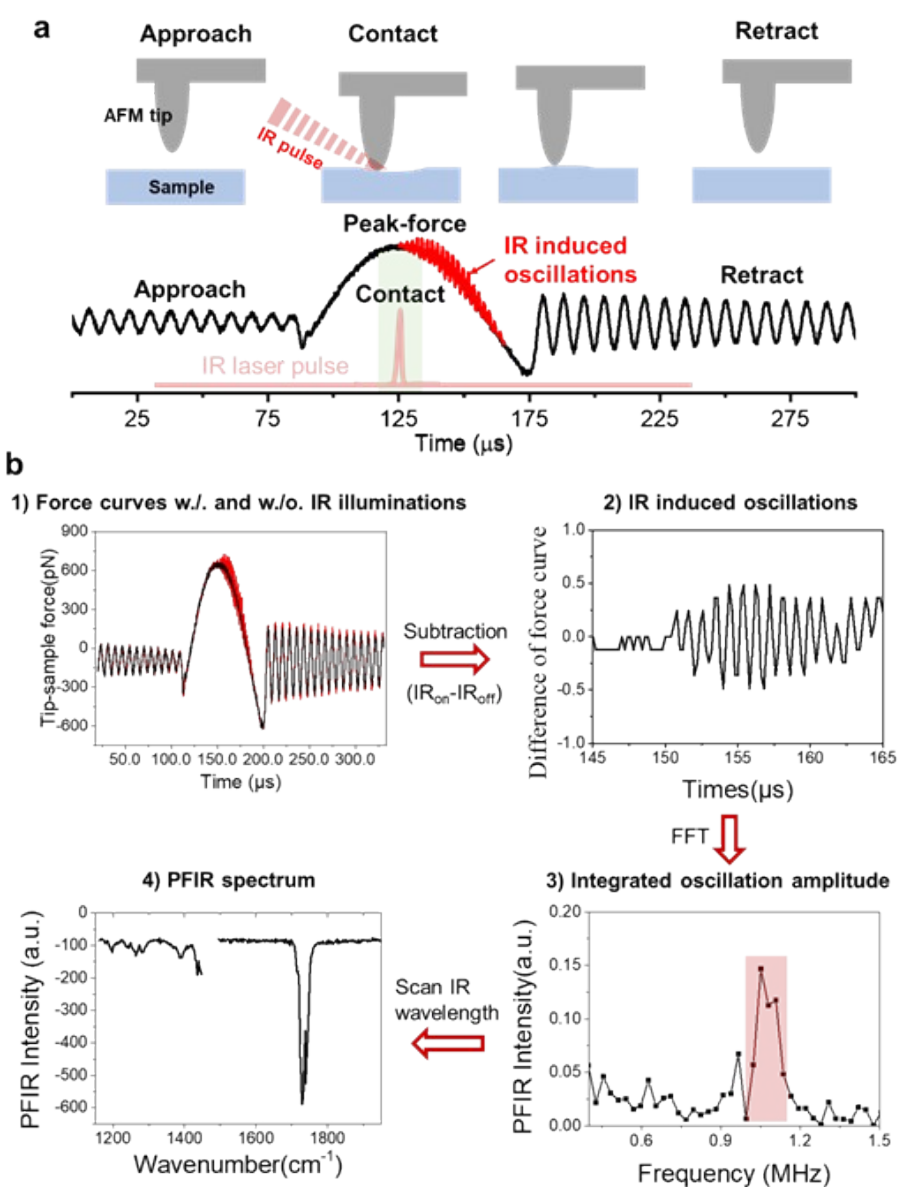
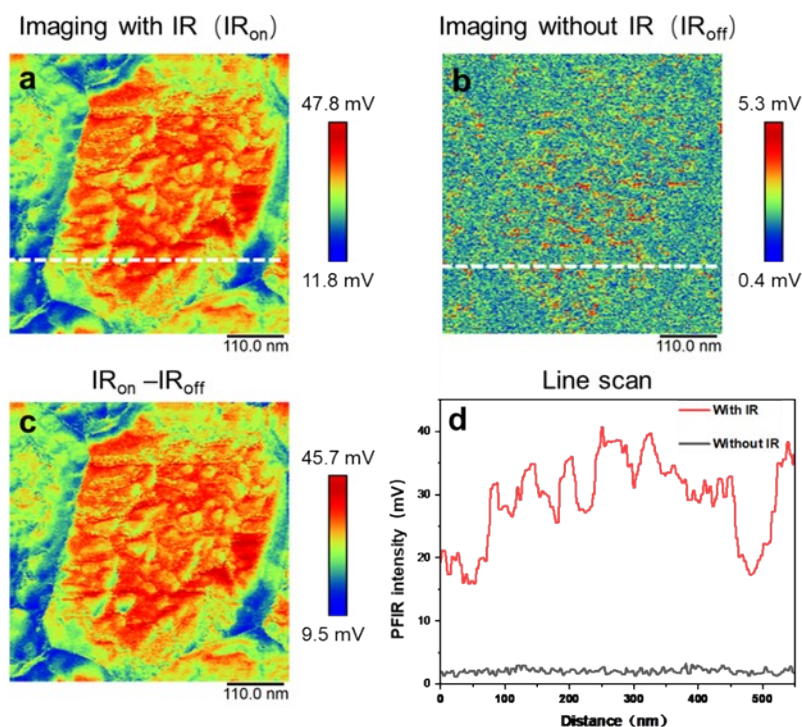


## Supporting Information

**Table S1** Assignment of Peak Positions in FTIR of Perovskite Thin Films.

Description of bands	Absorption( $\text{cm}^{-1}$ )
Rocking $\text{CH}_3\text{NH}_3$ (MA)	908
Rocking $\text{NH}_2$ (FA)	1011
Twisting $\text{NH}_2$ (FA)	1049
Bending $\text{NH}_3$ (MA)	1470
Bending $\text{NH}_2$ (FA)	1616

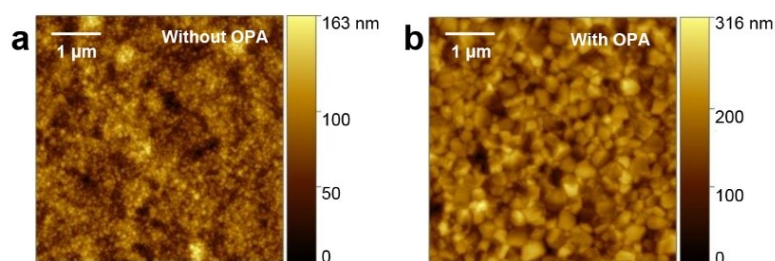




**Figure S2.** Comparison of imaging (a) with and (b) without IR illumination. The deduced imaging results is shown in (c). (d) PFIR spectra at labelled positions of white line in (a-b).

### Supplement on the mechanism of PFIR's work:

For the PFIR measurement, the IR light is applied only when the tip contacts the sample and the force between the tip and the sample reaches the peak-force region. The photothermal effect induced by the IR light causes sample expansion, exerting a force on the tip and inducing additional oscillations. Subtracting the force curves with and without IR light allows us to capture the IR absorption induced tip oscillations, in which the oscillation amplitude is proportional to the sample's IR absorption strength. By varying the wavelength of the incident IR light and repeating this process, we can compile a complete infrared spectrum. For imaging, we fix the wavelength of the excited IR light and scan different sample positions to measure absorption.



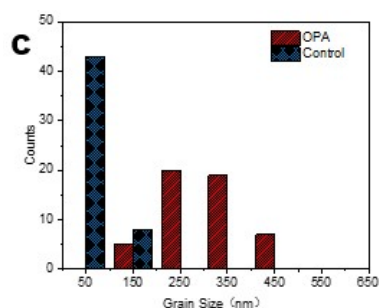


**Figure S3.** AFM morphology images of unmodified (a) and OPA-modified (b)  $\text{FA}_{0.9}\text{MA}_{0.05}\text{Cs}_{0.05}\text{PbI}_3$  perovskite. (c) Particle size distribution before and after OPA modification. The grain size of the unmodified perovskite is approximately 50-100 nm, whereas that of the OPA-modified perovskite lies in the region of 200-400 nm. The imaging range is 5  $\mu\text{m}$ .

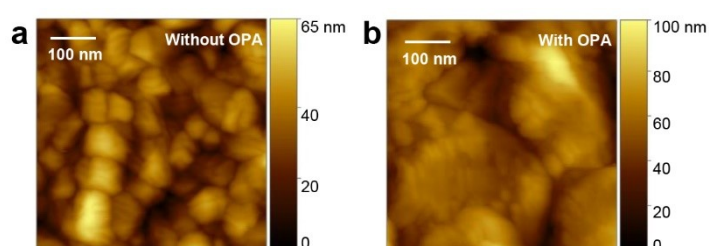


**Figure S4.** AFM morphology images of unmodified (a) and OPA-modified (b)  $\text{FA}_{0.9}\text{MA}_{0.05}\text{Cs}_{0.05}\text{PbI}_3$  perovskite. The surface of the unmodified perovskite grains exhibits striated texture, while the surface texture of the OPA-modified perovskite grains presents a mix of striations and block patterns. The imaging range is 500 nm.

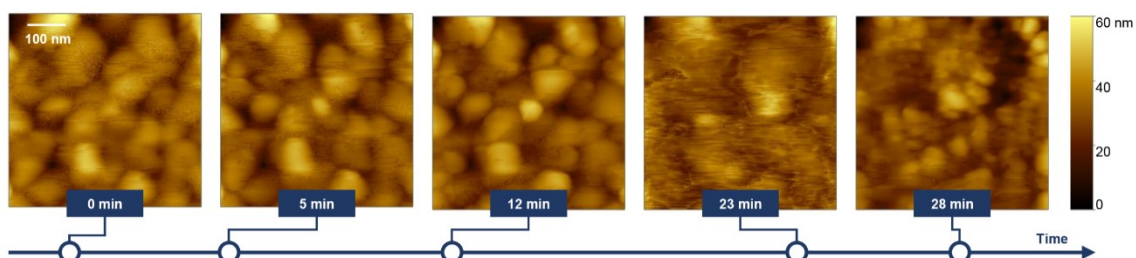


**Figure S5.** Consecutive imaging results from the same region of  $\text{FA}_{0.9}\text{MA}_{0.05}\text{Cs}_{0.05}\text{PbI}_3$  perovskite under high-power infrared laser, conducted five times. The scanning range is 500 nm. The quality of morphology imaging of the perovskite thin film visibly diminishes under high power, with the decline in the results after 23 minutes possibly due to probe contamination. There are notable morphological changes in the sample after 28 minutes, as compared to the initial morphology, with the emergence of smaller-sized grains.

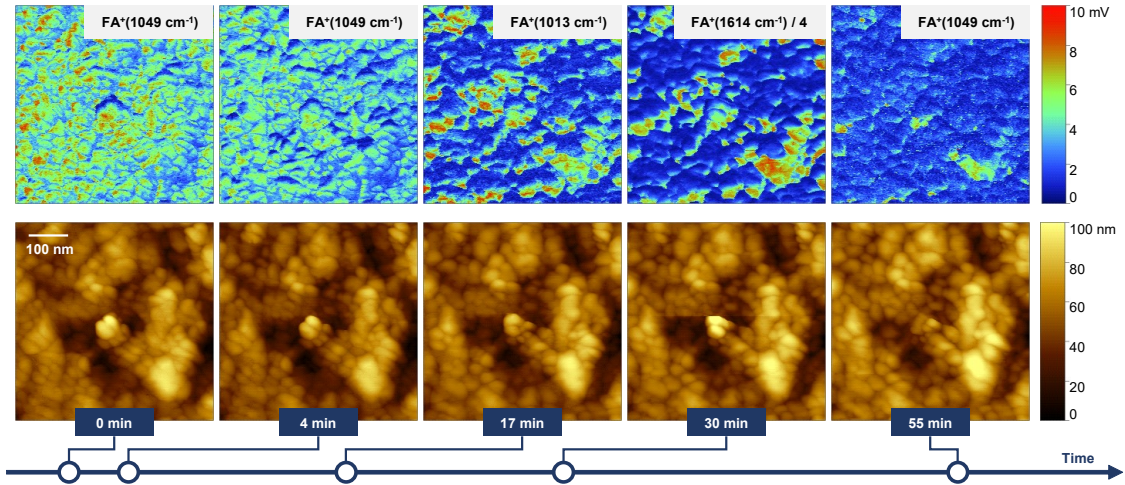


**Figure S6.** Continuous morphological and FA<sup>+</sup> imaging results from the same region of FA<sub>0.9</sub>MA<sub>0.05</sub>Cs<sub>0.05</sub>PbI<sub>3</sub> perovskite under high-power infrared laser. The imaging results at 0 minutes demonstrate the fresh perovskite morphology and FA<sup>+</sup> distribution, which is relatively uniform, with FA<sup>+</sup> loss observed only at grain boundaries and a few localized grain boundary areas. In the 17-minute imaging, a significant number of particle surfaces gradually start losing FA<sup>+</sup>. By the 55-minute mark, only a handful of grain surfaces still contain FA<sup>+</sup>. In characterizing the FA<sup>+</sup> distribution of the samples, we compared imaging under infrared light excitation for different FA<sup>+</sup> characteristic absorptions (1049 cm<sup>-1</sup>, 1013 cm<sup>-1</sup>, and 1614 cm<sup>-1</sup>). The infrared signal is strongest under 1614 cm<sup>-1</sup> excitation; for comparison, the infrared signal was reduced fourfold. The good consistency in FA<sup>+</sup> distribution under different wavelength excitations confirms the accuracy of nano-infrared imaging technology.

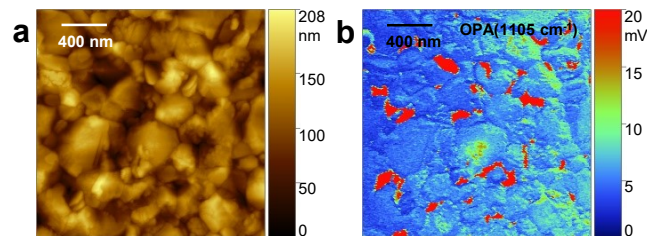


**Figure S7.** Chemical distribution of OPA in FA<sub>0.9</sub>MA<sub>0.05</sub>Cs<sub>0.05</sub>PbI<sub>3</sub> perovskite thin film. (a) Morphology of the perovskite, (b) Chemical imaging of OPA. Notable OPA signals are detected at the grain boundaries of the perovskite, with weaker OPA signals present on some grain surfaces.

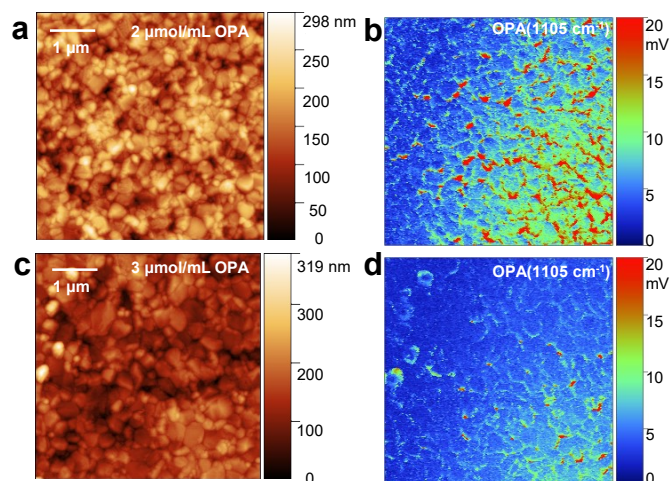


**Figure S8.** Comparison of perovskite thin films modified by OPA at different concentrations. (a) Morphology of the perovskite modified with 2  $\mu\text{mol/L}$  OPA, (b) OPA distribution corresponding to (a). (c) Morphology of the perovskite modified with 3  $\mu\text{mol/L}$  OPA, (d) OPA distribution corresponding to (c). The perovskite thin film with an OPA concentration of 3  $\mu\text{mol/L}$  has larger grain sizes than the perovskite thin film with an OPA concentration of 2  $\mu\text{mol/L}$ , but the uniformity of OPA distribution is poorer.

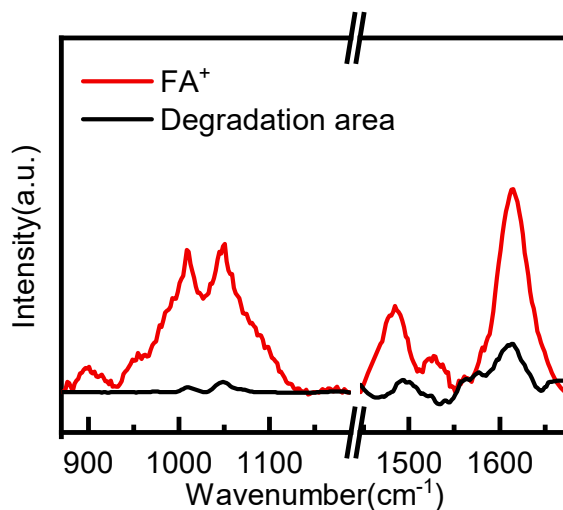


**Figure S9.** Comparison of nano-infrared spectra at different locations of  $\text{FA}_{0.9}\text{MA}_{0.05}\text{Cs}_{0.05}\text{PbI}_3$  perovskite thin film. The nano-infrared spectra of the  $\text{FA}^+$  locations and degraded sites marked in Figure 3b were compared. The organic content at the degradation sites is significantly reduced.

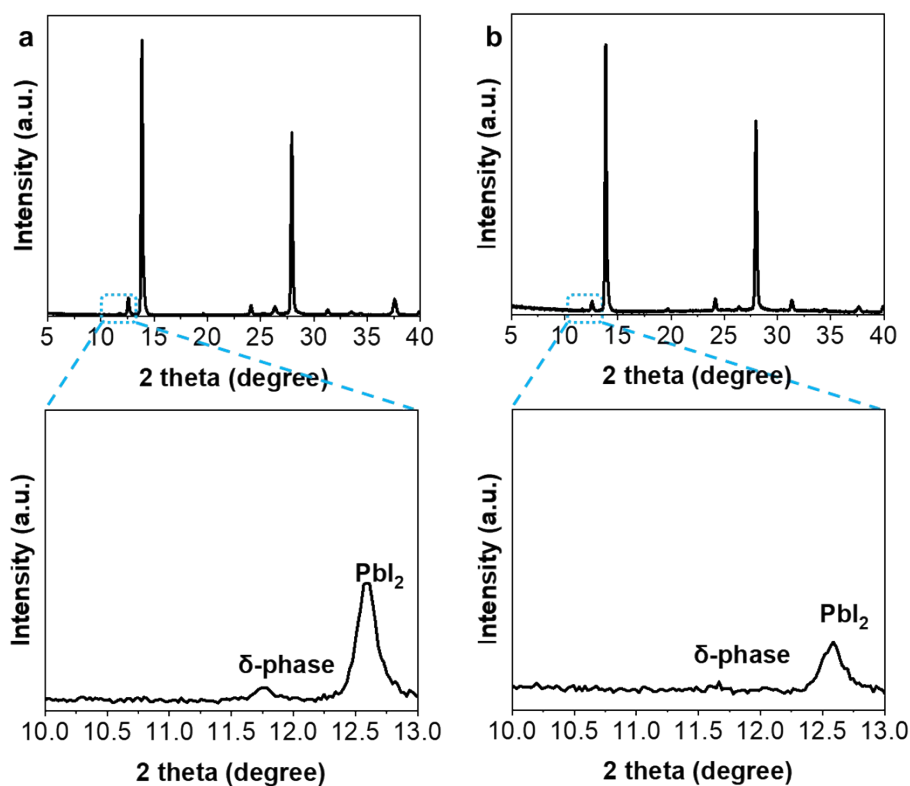


**Figure S10.** XRD of the perovskite films before and after aging, (a) unmodified perovskite, (b) OPA-modified perovskite. The picture mainly shows the red box part in the attached figure, and the 2 theta ranges from 10 to 13.

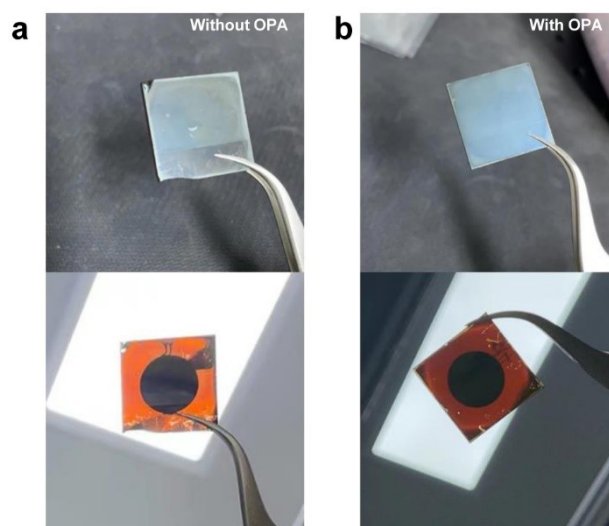


**Figure S11.** Photographs of the perovskite films after aging, (a) front and back of the unmodified perovskite, (b) front and back of the OPA-modified perovskite. The center of the back of both samples is covered by a black circular pad.  $\alpha$ -FAPbI<sub>3</sub> is black,  $\delta$ -FAPbI<sub>3</sub> is yellow; the phase transition is more pronounced in the unpassivated sample.